Quantum-enhanced distributed phase sensing with a truncated SU(1,1) interferometer

Seongjin Hong,[1,2,*] Matthew A. Feldman,[3,4] Claire E. Marvinney,[3,4] Donghwa Lee,[5] Changhyoup Lee,[6] Michael T. Febbraro,[1] Alberto M. Marino,[3,4,†] and Raphael C. Pooser[3,4]

[1]*Physical Sciences Division, Oak Ridge National Laboratory, Oak Ridge, Tennessee 37831, USA*
[2]*Department of Physics, Yonsei University, Seoul 03722, Korea*
[3]*Quantum Information Science Section, Computational Sciences and Engineering Division, Oak Ridge National Laboratory, Oak Ridge, Tennessee 37831, USA*
[4]*Quantum Science Center, Oak Ridge National Laboratory, Oak Ridge, Tennessee 37831, USA*
[5]*Center for Quantum Information, Korea Institute of Science and Technology, Seoul 02792, Korea*
[6]*Korea Research Institute of Standards and Science, Daejeon 34113, Korea*

(Received 13 May 2024; accepted 11 May 2025; published 5 June 2025)

In recent years, distributed quantum sensing has gained interest for a range of applications requiring networks of sensors, from global-scale clock synchronization to high energy physics. In particular, a network of entangled sensors can improve not only the sensitivity beyond the shot noise limit, but also enable a Heisenberg scaling with the number of sensors. Here, using bright entangled twin beams, we theoretically and experimentally demonstrate the detection of a linear combination of two distributed phases beyond the shot noise limit with a truncated SU(1,1) interferometer. Specifically, we show a quantum noise reduction of 1.7 ± 0.3 dB below what is possible with the corresponding classical configuration. Additionally, we theoretically extend the use of a truncated SU(1,1) interferometer to a multi-phase-distributed sensing scheme that leverages entanglement as a resource to achieve a quantum improvement in the scaling with the number of sensors in the network. Our results pave the way for developing quantum-enhanced sensor networks that can achieve an entanglement-enhanced sensitivity.

DOI: 10.1103/PhysRevResearch.7.023231

I. INTRODUCTION

Quantum metrology allows us to estimate an unknown parameter with enhanced sensitivity over classical approaches by exploiting quantum resources [1–7]. Quantum sensors that use entanglement or other quantum correlations provide a promising platform that has been used in a variety of sensing scenarios [8–10], from optomechanical sensors [11–13] to proposed dark matter detectors [14,15]. More recent developments in quantum metrology have been directed towards multi-parameter estimation techniques for various applications such as imaging, microscopy, and sensor networks [16–21]. In the case of a network of sensors, the goal of distributed quantum sensing is to measure the linear combination of spatially distributed parameters beyond the shot noise limit (SNL) [22–27]. Distributed quantum sensing has already been shown to provide advantages for applications such as local beam tracking and global-scale clock synchronization [28,29]. Moreover, recent proposals point to further sensitivity improvements from entanglement-enhanced arrays of distributed optical sensors for phase sensing, which could enable the detection of ultraweak signals in high energy physics, such as enhanced gravitational wave detection and detection of dark matter [13–15,30–32].

One approach for quantum-enhanced phase sensing is the use of a nonlinear interferometer, such as an SU(1,1) interferometer, where nonlinear amplifiers replace the beamsplitters in a standard SU(2) interferometer [33–35]. In these devices, entanglement is present inside the interferometer between the two optical paths and the nature of the quantum correlations requires the measurement of a linear combination of observables, such as the sum of the phase quadratures or the difference of the amplitude quadratures, in order to obtain the quantum noise reduction necessary to surpass the SNL. The SU(1,1) interferometer offers the potential to outperform its classical counterparts by a factor proportional to the nonlinear gain of the nonlinear amplifiers. Additionally, when seeded, the SU(1,1) interferometer can take advantage of the increased sensitivity due to the large number of photons that are used to perform the estimation [35,36].

A modified version of the SU(1,1) interferometer, the truncated SU(1,1) interferometer (tSU(1,1) interferometer), replaces the second nonlinear amplifier with two local balanced homodyne detectors, while obtaining the same quantum advantage of a full SU(1,1) interferometer [9,35]. Given that optical interference of the beams after sensing the parameter of interest is not needed with the tSU(1,1), it offers a natural

*Contact author: shong@yonsei.ac.kr
†Contact author: marinoa@ornl.gov

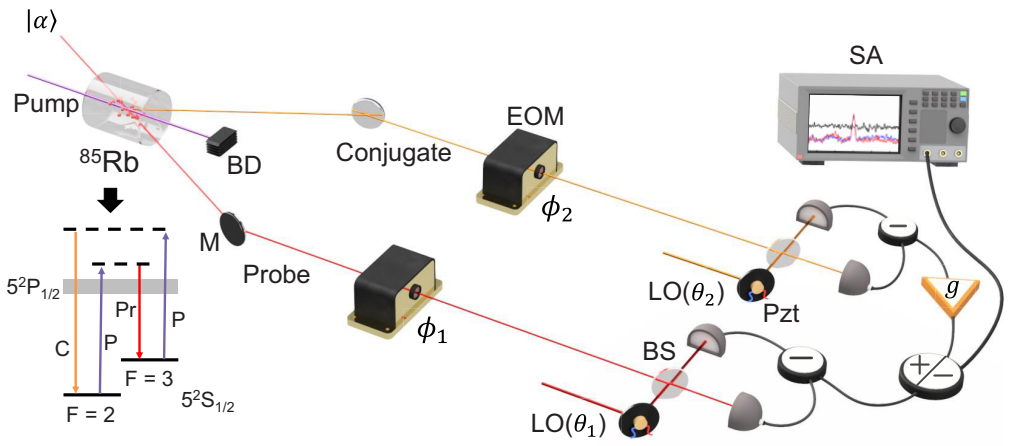

FIG. 1. Experimental setup to estimate the linear combination of two distributed phases in a tSU(1,1) interferometer. Bright two-mode squeezed states are generated by seeding a four-wave mixing process in a ^{85}Rb vapor cell with a weak coherent state. Each of the modes of the two-mode squeezed state experiences a phase shift, ϕ_1 and ϕ_2, respectively. The two modes are then measured with two homodyne detectors to perform a joint measurement to estimate $\phi = \beta_1\phi_1 + \beta_2\phi_2$. BD: beam dump; M: mirror; EOM: electro-optic modulator; LO: local oscillator; BS: beamsplitter; PZT: piezoactuator; SA: spectrum analyzer.

way to implement a distributed quantum sensor to measure two distributed phases, one in each of the two entangled arms of the interferometer. Despite these advantages such as entanglement between two paths, the large number of photons, and local measurements, the tSU(1,1) has previously only been used to measure a single-phase along one of its arms [8,12,35], and its application to distributed quantum sensing has remained largely unexplored. Here, we introduce the use of the tSU(1,1) interferometer for distributed quantum phase sensing, demonstrating its ability to measure two distributed phases simultaneously. Additionally, the presence of entanglement in this system has the potential to improve the scaling of the distributed sensor when extending beyond two phases.

In this paper, we theoretically and experimentally study the use of two-mode squeezed states in a distributed quantum sensor to measure the linear combination of two phases with a quantum-enhanced phase sensitivity. For the experimental two-phase distributed sensing, we achieve a quantum noise reduction of 1.7 ± 0.3 dB beyond the SNL when using a distributed two-mode squeezed light source in a tSU(1,1) interferometer configuration. This allows us to experimentally demonstrate that signals hidden in the noise in the classical sensing approach become observable when measured with the tSU(1,1) interferometer. We additionally extend the theory to study entanglement-enhanced distributed phase sensing for M distributed phases. To this end, we consider a beamsplitter network to extend from a two-mode entangled state to a multimode entangled state and show that an additional entanglement-enhanced phase sensitivity can be achieved over that of an optimal distributed sensor network probed with separable quantum states. We theoretically demonstrate the expected Heisenberg sensitivity scaling with the number of sensors and show that the tSU(1,1) interferometer has the potential to surpass practical classical approaches with bright two-mode squeezed light in a distributed sensor network that enables an entanglement-enhanced sensitivity beyond the SNL.

II. DISTRIBUTED QUANTUM SENSING WITH A TRUNCATED SU(1,1) INTERFEROMETER

Our initial goal is to demonstrate a distributed quantum sensing configuration that can measure a linear combination of two distributed phases beyond the SNL with a two-mode squeezed state, as shown in the experimental schematic in Fig. 1. We start by considering two unknown phases, ϕ_1 and ϕ_2, that are distributed in different locations, with the goal of estimating the linear combination $\phi = \beta_1\phi_1 + \beta_2\phi_2$, with the normalization condition $|\beta_1| + |\beta_2| = 1$ [37,38].

In general, the phase sensitivity of a measurement, $\Delta\phi$, can be evaluated from the signal-to-noise ratio (SNR), which is given by

$$\mathrm{SNR} = \frac{(\partial_\phi \langle \hat{X}_+ \rangle)^2}{\Delta^2 X_+} \Delta^2\phi, \tag{1}$$

where $\hat{X}_+$ represents an observable and $\Delta^2 X_+$ describes the variance of the measurement, i.e., $\Delta^2 X_+ = \langle \hat{X}_+^2 \rangle - \langle \hat{X}_+ \rangle^2$ [8,9,12,35]. The minimum detectable phase shift is then determined when the SNR $= 1$. We thus define the measurement sensitivity as [8,39]

$$\Delta^2\phi = \frac{\Delta^2 X_+}{(\partial_\phi \langle \hat{X}_+ \rangle)^2}. \tag{2}$$

Here, we analyze the measurement sensitivity of the distributed sensing configuration in a tSU(1,1) interferometer in the limit of bright quantum states of light, which can enable the extension of the sensing configuration to practical applications.

In our configuration, bright two-mode squeezed light is generated as part of the tSU(1,1) interferometer. A four-wave mixing (FWM) process in a double-lambda scheme in a ^{85}Rb vapor (see inset in Fig. 1) [40,41] is used to generate the required two-mode squeezed states. To generate bright beams, the probe beam for the FWM is weakly seeded with a coherent state with an average photon number $|\alpha|^2$. This then leads to the generation of an amplified probe with a photon number of

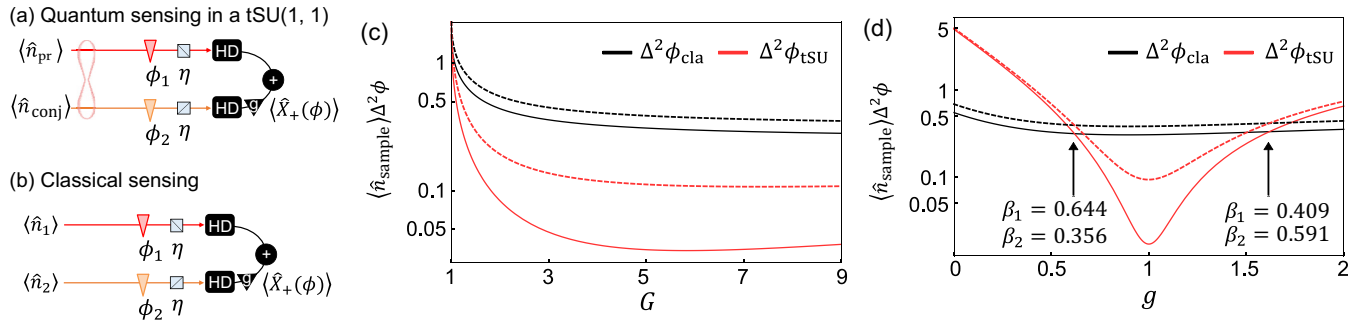

FIG. 2. Comparison of (a) distributed quantum sensing in a tSU(1, 1) and (b) classical sensing approaches. To obtain a fair comparison between the sensitivities for the two schemes, the total optical power that interacts with the phase elements is held constant, i.e., $\langle\hat{n}_{pr}\rangle = \langle\hat{n}_1\rangle$ and $\langle\hat{n}_{conj}\rangle = \langle\hat{n}_2\rangle$. (c) Measurement sensitivities multiplied by the total number of photons probing the phase elements, $\langle\hat{n}_{sample}\rangle = \langle\hat{n}_{pr}\rangle + \langle\hat{n}_{conj}\rangle$, for the two sensing approaches as a function of gain G when $\beta_1 = \beta_2 = 1/2$. The solid traces correspond to the lossless case, with $\eta = 1$, while the dashed traces correspond to the case with some loss, specifically with $\eta = 0.8$. (d) Measurement sensitivities multiplied by $\langle\hat{n}_{sample}\rangle$ for the same two cases shown in (c) as a function of the classical gain factor g when $G = 5$ for the lossless case ($\eta = 1$, solid lines) and the case with losses ($\eta = 0.8$, dashed lines). A quantum-enhanced sensitivity can be achieved from $g = 0.618$ to $g = 1.618$ in the lossless case, which translates to a linear phase superposition of $\phi = 0.644\phi_1 + 0.356\phi_2$ and $\phi = 0.409\phi_1 + 0.591\phi_2$, respectively. HD: homodyne detection.

$G|\alpha|^2 + (G-1)$ and a corresponding conjugate beam with a photon number of $(G-1)|\alpha|^2 + (G-1)$, where the $(G-1)$ term is due to spontaneous FWM while the terms proportional to $|\alpha|^2$ result from the stimulated process. In the case of $|\alpha|^2 \gg 1$ the stimulated process dominates and the mean photon numbers can be approximated as $G|\alpha|^2$ and $(G-1)|\alpha|^2$, respectively. In these equations, G is the gain of the nonlinear interaction and is related to the squeezing parameter according to $r = \cosh^{-1}(\sqrt{G})$.

After the FWM process, phase shifts ϕ_1 and ϕ_2 are imparted on the probe and conjugate beams, respectively. The probe and conjugate are then sent to balanced homodyne detectors with local oscillator (LO) phases θ_1 and θ_2, respectively, to measure the corresponding generalized quadrature operators, $\hat{X}_1(\phi_1, \theta_1)$ and $\hat{X}_2(\phi_2, \theta_2)$, which are defined in Appendix A. To simplify the notation, we focus on the LO phases that provide the optimal measurement sensitivity, specifically $\theta_1 = \theta_2 = \pi/2$, that correspond to measurements of the phase quadratures, and drop the θ dependence throughout the manuscript. To obtain an estimate of the linear combination of the unknown phases (ϕ), we define the operator $\hat{X}_+$ such that $\hat{X}_+(\phi) = \hat{X}_1(\phi_1) + g\hat{X}_2(\phi_2)$, with g representing a classical gain factor to scale the homodyne detection of $\hat{X}_2(\phi_2)$ [42,43]. When losses are accounted for, one obtains (see Appendix A)

$$\begin{aligned}\langle\hat{X}_+(\phi)\rangle &= 2\alpha\sqrt{\eta}[\sqrt{G}\sin(\phi_1) + g\sqrt{G-1}\sin(\phi_2)]\\ &\approx 2\alpha\sqrt{\eta}(\sqrt{G}\phi_1 + g\sqrt{G-1}\phi_2)\\ &= 2\alpha\sqrt{\eta}(\sqrt{G} + g\sqrt{G-1})\phi, \end{aligned} \tag{3}$$

where $\eta \in [0, 1]$ is the transmission through the system, such that $\eta = 1$ indicates no loss. In deriving this result we made the assumption that the losses on the probe and conjugate are the same and that ϕ_1 and ϕ_2 are small, such that $\sin(\phi_i) \approx \phi_i$. Additionally, the weighting factors, β_1 and β_2, of the two terms in the linear combination of phases, $\phi = \beta_1\phi_1 + \beta_2\phi_2$, are defined as $\beta_1 = \sqrt{G}/(\sqrt{G} + g\sqrt{G-1})$ and $\beta_2 = g\sqrt{G-1}/(\sqrt{G} + g\sqrt{G-1})$. Putting all of this together, the measurement sensitivity for our sensing approach with a tSU(1,1) interferometer to sense the linear combination of two phases is theoretically calculated to be

$$\Delta^2\phi_{tSU} = \frac{(g^2+1)(1-2\eta+2\eta G) - 4g\eta\sqrt{G(G-1)}}{4|\alpha|^2\eta(\sqrt{G} + g\sqrt{G-1})^2}. \tag{4}$$

We also calculate the quantum Cramér-Rao bound (QCRB) for our configuration to be $\Delta^2\phi_{QCRB} = (1 - 2\eta + 2\eta G - 2\eta\sqrt{G(G-1)})/(2|\alpha|^2\eta(\sqrt{G} + \sqrt{G-1})^2)$, as outlined in Appendix A [42,43]. As can be seen, the measurement sensitivity given by Eq. (4) saturates the QCRB for $g = 1$, which means that the measurement is optimal [42–44].

Next, we compare the sensitivity of the distributed sensing approach in which phase shifts are simultaneously present in both arms of the tSU(1,1) interferometer with the corresponding classical sensing approach, as shown in Figs. 2(a) and 2(b), respectively. For these cases, the total phase shift for each phase element was kept constant, which we believe closely resembles what would happen in an actual experiment where one is trying to measure a signal, such as a gravitational wave, that is spatially distributed [13,30–32]. To have a fair comparison between the classical and quantum configurations, we take the resources in the estimation to be the number of photons probing the phase elements. In the quantum scheme, $\langle\hat{n}_{pr}\rangle = G|\alpha|^2$ and $\langle\hat{n}_{conj}\rangle = (G-1)|\alpha|^2$ interact with ϕ_1 and ϕ_2, respectively. Similarly, in the classical scheme, $\langle\hat{n}_1\rangle$ and $\langle\hat{n}_2\rangle$ interact with ϕ_1 and ϕ_2, respectively. These photon numbers are kept at a constant value for all cases, i.e., $\langle\hat{n}_{pr}\rangle = \langle\hat{n}_1\rangle$ and $\langle\hat{n}_{conj}\rangle = \langle\hat{n}_2\rangle$. Under these conditions, the measurement sensitivity for the classical approach can be shown to be given by $\Delta^2\phi_{cla} = (1+g^2)/(4|\alpha|^2\eta(\sqrt{G} + g\sqrt{G-1}))$.

Figure 2(c) shows the theoretically calculated measurement sensitivity multiplied by the total number of photons probing the phase elements, $\langle\hat{n}_{sample}\rangle = \langle\hat{n}_{pr}\rangle + \langle\hat{n}_{conj}\rangle$, as a function of gain (G) with $\eta = 1$ (solid lines) and $\eta = 0.8$ (dashed lines) when $\beta_1 = \beta_2 = 1/2$. There is a clear quantum-enhanced sensitivity for the distributed two-phase sensing with a tSU(1,1) interferometer over the corresponding classical approach. In addition, we calculate the normalized measurement sensitivity as a function of the classical gain factor g when $G = 5$, as shown in Fig. 2(d). A quantum-enhanced

sensitivity over that of the corresponding classical benchmark can be obtained in the range of $0.618 < g < 1.618$, which translates to an adjustment of ϕ from $\phi = 0.644\phi_1 + 0.356\phi_2$ to $\phi = 0.409\phi_1 + 0.591\phi_2$. Note that the weightings between phases ϕ_1 and ϕ_2 are adjustable while still maintaining a certain amount of quantum noise reduction in the sensor even without optimizing g. Further details on the sensitivity calculations can be found in Appendix A.

III. EXPERIMENTAL RESULTS

The tSU(1,1) interferometer used for our distributed sensing experiments uses a two-mode squeezed light state generated with a FWM process in a ^{85}Rb vapor cell (see Appendix D for details) to probe two independent phase shifts, as shown in Fig. 1. As noted previously, this configuration can be used for distributed sensing as there is no need to optically interfere the two modes after interfacing with the phase elements. For our experiment, a strong (360 mW) pump beam and a weak (5 μW) probe seed beam (redshifted by 3.044 GHz from the frequency of the pump) are mixed at an angle of 0.3° in a 12.7 mm long ^{85}Rb vapor cell, which is heated to 100 °C. The pump and probe have beam diameters of 920 μm and 560 μm, respectively. This configuration leads to a gain of $G \approx 5$, such that seeding the probe beam leads to an optical power for the probe and conjugate beams of 26 μW (an average of 10×10^{13} photons) and 17 μW (an average of 6.8×10^{13} photons), respectively. These power levels are kept constant for all experiments and used to probe the phase elements. Note that the generated bright beams of light have significantly larger optical power than squeezed vacuum states or Fock states and thus they can be applied to practical sensing applications requiring few tens of microwatts or higher powers [4].

To ensure an optimal spatial mode matching for the homodyne measurements, we generate the required LOs with a second independent FWM process (not shown in Fig. 1) as described in Appendix D. For this, a coherent state with 44.5 μW is also injected into the same vapor cell and mixed with its own pump beam in order to generate an LO pair with matching spatial mode properties to those of the probe and conjugate beams [45]. The LOs also experience gain in the cell, leading to optical powers approximately an order of magnitude larger than their respective probe and conjugate beams due to the larger seed power. For homodyne detection, the probe and conjugate are interfered with their respective LOs, after which they are independently detected with a difference measurement using a pair of balanced photodiodes. The external phase references are set by the LOs, such that the probe and conjugate are locked with a $\pi/2$ phase offset with respect to these references to measure phase squeezing (for details on the LO lock see Appendix D). The observable $\hat{X}_+(\phi)$ is then measured using a hybrid junction to obtain the sum of the signals from the dual balanced homodyne detectors and read out with a spectrum analyzer (SA).

Before detection, phase shifts at a frequency of 300 kHz are imparted on the two-mode squeezed state using two electro-optic modulators (EOMs), as shown in Fig. 1. The signal resulting from the 300 kHz modulation appears as a peak on the SA. The SNL for all signals is measured with the same setup when only the order of magnitude larger LOs are incident on the balanced detectors and the squeezed light is blocked.

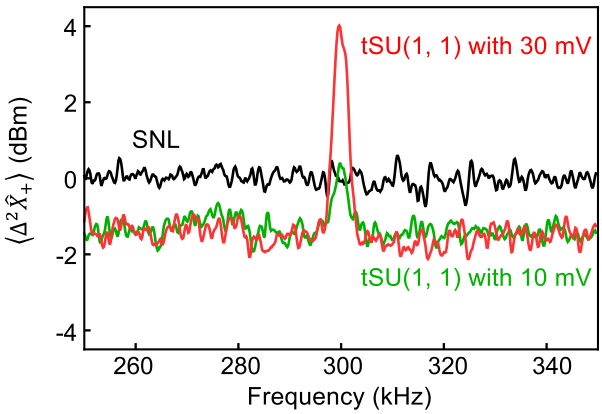

FIG. 3. Measured spectrum analyzer traces. The red and green lines indicate the quantum sensing approach in a tSU(1,1) when driving the EOMs with signal amplitudes of 30 mV and 10 mV at 300 kHz, respectively. The black line represents the corresponding SNL. A quantum noise reduction of 1.7 ± 0.3 dB relative to the SNL is achieved. Settings for the spectrum analyzer: resolution bandwidth (RBW) = 3 kHz; video bandwidth (VBW) = 100 Hz; sweep time = 1 s. All traces are averaged 15 times.

In the experiment, we set the phases along each arm of the interferometer to the same value $\phi = \phi_1 = \phi_2$ and β_1 and β_2 are set to $1/2$ by adjusting the classical gain g. We apply both phase shifts simultaneously along each optical path, as shown in Fig. 2(a). The measured signals are shown in Fig. 3, with the red (large signal) and green (small signal) traces corresponding to the tSU(1, 1) approach with two-mode squeezed states and the black trace corresponding to the SNL. As can be seen, for the quantum approach a 1.7 ± 0.3 dB quantum enhancement with respect to the corresponding SNL was achieved. As a result, small signals are only observable when using the quantum approach, as shown in Fig. 3 by the green trace, which illustrates the usefulness of the tSU(1,1) for distributed sensing.

IV. DISTRIBUTED MULTIPHASE SENSING WITH A tSU(1,1) INTERFEROMETER

We now extend the theory developed for the case of two distributed phases with a tSU(1,1) interferometer to that of a generalized configuration for sensing M distributed phases with M entangled probe beams in a tSU(1,1) interferometer. In Ref. [24], it has been theoretically and experimentally proposed that Heisenberg scaling for both the average photon number and the number of sensors, each probed by a separate mode, can be achieved in distributed quantum sensing using a single-mode squeezed state and a beamsplitter array. Here we show that the two-mode squeezed states that were the basis for our experiments can also be used to generate a multimode entangled state by utilizing a balanced beamsplitter network (BSN) consisting of beamsplitter arrays, similar to those in Refs. [22,24]. The multimode entangled state can then be used to measure a linear combination of M phases. Here, we

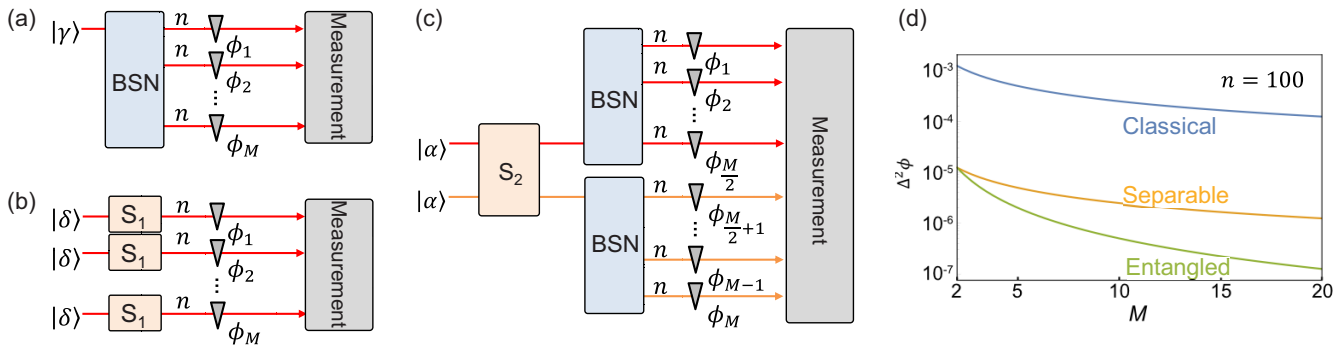

FIG. 4. Schemes for distributed sensing of a linear superposition of M unknown phases with (a) a classical sensing scheme, (b) a separable scheme composed of multiple independent single-mode squeezed states, and (c) a multimode entangled scheme based on a two-mode squeezed state in a tSU(1,1) interferometer. The average photon number n, which is incident on each phase element, is kept fixed for all the schemes. (d) Theoretical prediction for the measurement sensitivity, in the case of no loss, as a function of the number of unknown phases (M) for $n = 100$. Blue, orange, and green solid lines indicate the measurement sensitivity for the classical, separable, and entangled schemes, respectively. As can be seen, the entangled scheme has a better sensitivity than the other schemes for the estimation of the average of the distributed phases. S_1: single-mode squeezing operator; S_2: two-mode squeezing operator; BSN: beamsplitter network.

consider the average of the phases, i.e., $\phi = \sum_{j=1}^{M} \phi_j/M$, with M being the number of unknown phases.

We compare the measurement sensitivities for the measurement of the average of M unknown phases for the three cases shown in Figs. 4(a) through 4(c): a classical scheme, a separable scheme composed of multiple independent single-mode squeezed states [24], and the multimode entangled scheme with the two-mode squeezed states in a tSU(1,1) interferometer, respectively. For the theoretical analysis, we consider the optimal separable configuration, as shown in [24], to better illustrate the quantum advantage from entanglement of the proposed scheme. Finally, we constrain the average photon number, n, incident on each phase element to be constant for all three schemes. This is done by appropriately setting the input seed powers for the three cases (i.e., $|\gamma|^2$, $|\delta|^2$, and $|\alpha|^2$).

More specifically, the classical scheme consists of a coherent state as the input to a BSN, which is used to distribute it to M phases elements that impart phase shifts ϕ_1 to ϕ_M prior to a joint measurement. The separable scheme consists of M single-mode squeezed states that independently probe M distributed phases prior to a joint measurement. Finally, for the M mode entangled case, BSNs are used to distribute a two-mode squeezed state to probe the M distributed phase elements. In order to balance the power equally among the M phase elements, we consider the case in which both probe and conjugate beams of the tSU(1,1) are weakly seeded with a coherent state with mean photon number $|\alpha|^2$, such that the total number of photons prior to the BSNs is equal to $N_{\text{tot}} = 2(G-1) + 4G|\alpha|^2 + 2|\alpha|^2(-1 + 2\sqrt{G(G-1)})$, where G is the nonlinear gain. The BSNs split the two-mode squeezed state into $2d = M$ modes, such that the average photon number probing each phase element is equal to $n = N_{\text{tot}}/M$ prior to detection with a joint measurement.

For all three schemes, we calculate the measurement sensitivity when all phase elements introduce the same phase shift, $\phi_1 = \phi_2 = \cdots = \phi_M = \phi$, as a function of both n and M for the lossless case with $\eta = 1$. Given this, we find that the optimal sensitivities for each scheme take the form

$$\Delta^2\phi_{\text{cla}} = \frac{1}{4Mn}, \tag{5}$$

$$\Delta^2\phi_{\text{sep}} = \frac{1}{4Mn(n+1)}, \tag{6}$$

$$\Delta^2\phi_{\text{ent}} = \frac{1}{2Mn(Mn+2)}. \tag{7}$$

Full details of the calculation for the multimode entangled scheme for distributed sensing in a tSU(1,1) interferometer can be found in Appendix C, along with the required calculations for determining the measurement sensitivity for the other two schemes.

Notably, we find that, while the separable case with quantum resources achieves a Heisenberg scaling with the number of photons, the entangled scheme with a tSU(1,1) interferometer achieves Heisenberg scaling with both the average photon number n and the number of modes M. Figure 4(d) shows the measurement sensitivities for all three cases as a function of the number of unknown phases M for the lossless case with an average photon number $n = 100$. Both schemes with quantum resources show a significant improvement in their measurement sensitivity in comparison to the classical scheme. Additionally, when more than two phases are sensed in the distributed sensor network, there is a clear improvement in sensitivity when using the entangled scheme in a tSU(1,1) interferometer over that of using the separable scheme, thus demonstrating that an additional entanglement-enhanced sensitivity is possible.

We emphasize that our results provide useful guidelines for practical application toward long-distance sensor networks. One promising direction is exploiting state-of-the-art long-distance entanglement distribution by applying techniques such as high-efficiency coupling of two-mode squeezed states into optical fibers and using low-loss antiresonant hollow core fibers [46,47]. Additionally, exploring the use of quantum memory for long-distance distribution, particularly with bright, resonant two-mode squeezed states in alkali atoms,

could be another interesting direction for future research [48]. By employing these techniques to multimode entangled states across multiple modes, it would be possible to measure a linear combination of multiple parameters across different modes in a long-distance sensor network. For long-distance distribution of multimode entanglement, multiplexing the LOs with the entangled state or locally generating them is required to enable proper detection at the network nodes [49,50]. Additionally, optimizing measurement sensitivity with respect to the squeezing level—while taking into account experimentally feasible limits—is crucial for near-term applications [51]. An extension of this work, beyond the scope of this paper, would be to study the quantum enhancement in distributed phase sensing using different entanglement resource states beyond those shown here. These entangled resources could include states such as dual-rail cluster states, which can be generated with an optical spatial mode comb [52].

V. CONCLUSION

We theoretically and experimentally investigate the measurement of a linear combination of distributed phases in a sensor network using bright quantum states of light. For the distributed sensing of two phases, both theory and experiment show that distributed phase sensing in a nonlinear interferometer provides a measurement sensitivity improvement over the corresponding classical sensing approach. In the experimental demonstration, the distributed sensing approach in a tSU(1,1) interferometer provides up to 1.7 dB of quantum noise reduction below the SNL. Further, we theoretically show that the distributed phase sensing scheme in a tSU(1,1) interferometer can be generalized to estimate the linear superposition of multiple phases with multimode entangled states. This generalized M mode entangled distributed phase sensor can be built by starting from the bright two-mode squeezed source used in our experiments. This approach provides an improved sensitivity scaling over that of the optimal separable distributed sensor using independent single-mode squeezed states of light. Our results pave the way for developing quantum-enhanced sensor networks that can provide a quantum advantage that also leverages entanglement for a range of sensing applications from global-scale clock synchronization to high energy physics, including applications that benefit from bright probing fields to obtain sensitivities that can go beyond the classical state of the art.

ACKNOWLEDGMENTS

S.H., R.C.P., M.T.F., and M.A.F. were supported by the U.S. DOE Office of Science, Office of High Energy Physics, QuantISED program (under Grant No. FWP ERKAP63). A.M.M. and C.E.M. received support from the U.S. DOE, Office of Science, National Quantum Information Science Research Centers, Quantum Science Center. S.H. and C.L. were supported by an Institute for Information & Communications Technology Planning & Evaluation (IITP) grant funded by the Korea government (MSIT) (Grant No. RS-2023-00222863) and S.H. was also supported by the National Research Foundation of Korea (NRF) (Grants No. RS-2023-00283146 and No. RS-2024-00352325). This manuscript has been authored, in part, by UT-Battelle LLC, under Contract No. DE-AC05-00OR22725 with the U.S. Department of Energy (DOE).

S.H. led the experimental effort and data analysis, R.C.P. oversaw the research, M.T.F. advised on the experiment, and M.A.F. assisted in building the experiment. A.M.M. oversaw the research and assisted with theory and data analysis and C.E.M. advised and assisted with data collection and experimental design. All authors contributed to the analysis and writing.

DATA AVAILABILITY

The publisher acknowledges the U.S. government license to provide public access under the DOE Public Access Plan [53].

APPENDIX A: PHASE SENSITIVITY CALCULATIONS

Here we derive the phase sensitivity for the distributed two-phase sensing approach considered for the experimental implementation. We consider the use of a tSU(1,1) interferometer as a distributed sensor, as shown schematically in Fig. 5(a). For the generation of the two-mode squeezed state, we consider two modes, $\hat{a}_0$ and $\hat{b}_0$, as the input for the parametric amplifier implemented with a FWM process. To model the phase insensitive configuration used in the experiment, mode $\hat{a}_0$ is taken to be a coherent state used as a weak probe seed, with $\langle \hat{a}_0^\dagger \hat{a}_0 \rangle = |\alpha|^2$, while mode $\hat{b}_0$ is taken to be a vacuum state, i.e., $\langle \hat{b}_0^\dagger \hat{b}_0 \rangle = 0$, as the conjugate is unseeded. In the ideal case, the FWM process in the ^{85}Rb vapor cell leads to a nonlinear gain, $G = \cosh^2(r)$, where r is the squeezing parameter, that transforms the input modes into output modes $\hat{a}_g$ and $\hat{b}_g$ for the probe and conjugate beams, respectively, according to [54]

$$\begin{pmatrix} \sqrt{G} & 0 & 0 & \sqrt{G-1} \\ 0 & \sqrt{G} & \sqrt{G-1} & 0 \\ G & \sqrt{G-1} & \sqrt{G} & 0 \\ \sqrt{G-1} & 0 & 0 & \sqrt{G} \end{pmatrix} \begin{pmatrix} \hat{a}_0 \\ \hat{a}_0^\dagger \\ \hat{b}_0 \\ \hat{b}_0^\dagger \end{pmatrix} = \begin{pmatrix} \hat{a}_g \\ \hat{a}_g^\dagger \\ \hat{b}_g \\ \hat{b}_g^\dagger \end{pmatrix}. \tag{A1}$$

After the FWM process, modes $\hat{a}_g$ and $\hat{b}_g$ interact with the phase elements to introduce phase shifts ϕ_1 and ϕ_2, respectively, to produce output modes $\hat{a}_p = e^{-i\phi_1}\hat{a}_g$ and $\hat{b}_p = e^{-i\phi_2}\hat{b}_g$. Additionally, optical losses in the paths of the beams need to be considered, which leads to the transformations $\hat{a}_f = \sqrt{\eta}\hat{a}_p + \sqrt{1-\eta}\hat{c}_0$ and $\hat{b}_f = \sqrt{\eta}\hat{b}_p + \sqrt{1-\eta}\hat{d}_0$, where we have considered the case of equal loss for both probe and conjugate beams. In this case, we model the loss with a beamsplitter transformation with transmission η (where $\eta = 1$ is the lossless case) for each of the beams with vacuum modes $\hat{c}_0$ and $\hat{d}_0$ coupling in through the unused input port of the beamsplitters in the probe and conjugate paths, respectively. Given that the FWM process is seeded with $|\alpha|^2 \gg 1$, the optical power of the probe and conjugate can be approximated as $\langle \hat{a}_f^\dagger \hat{a}_f \rangle = \eta(-1 + G + G|\alpha|^2) \approx \eta G|\alpha|^2$ and $\langle \hat{b}_f^\dagger \hat{b}_f \rangle = \eta(-1 + G + (G-1)|\alpha|^2) \approx \eta(G-1)|\alpha|^2$, respectively.

The modes after probing the phase elements, $\hat{a}_f$ and $\hat{b}_f$, are measured with two independent balanced homodyne

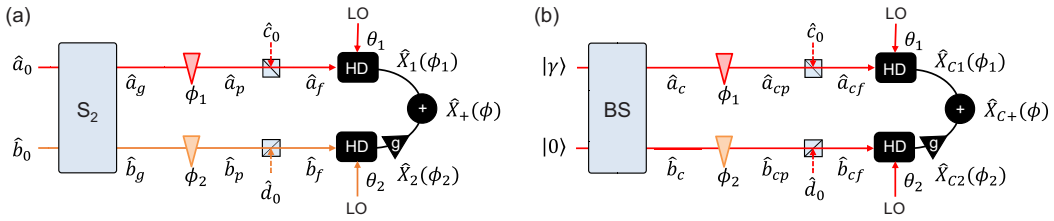

FIG. 5. Schematics for the models used to derive the phase sensitivity when using (a) a two-mode squeezed state in a tSU(1,1) interferometer and (b) the corresponding classical configuration. S_2: two-mode squeezing operator; BS: beamsplitter.

detectors that have LOs with phases θ_1 and θ_2, respectively, that serve as external phase references. We define generalized quadrature operators $\hat{X}_1(\phi_1,\theta_1) = e^{-i\theta_1}\hat{a}_f^\dagger + e^{i\theta_1}\hat{a}_f$ and $\hat{X}_2(\phi_2,\theta_2) = e^{-i\theta_2}\hat{b}_f^\dagger + e^{i\theta_2}\hat{b}_f$ for the probe and conjugate, respectively. These generalized quadratures are combined to obtain the joint quadrature operator $\hat{X}_+(\phi) = \hat{X}_1(\phi_1,\theta_1 = \pi/2) + g\hat{X}_2(\phi_2,\theta_1 = \pi/2)$, where g is a classical gain factor that provides a relative scaling between the probe and conjugate homodyne detectors and the external phase references given by the LOs are set to $\theta_1 = \theta_2 = \pi/2$ to perform measurements of the phase quadratures. In this case, the expectation value and variance for $\hat{X}_+$ are given by

$$\begin{aligned}\langle\hat{X}_+(\phi)\rangle &= 2\alpha\sqrt{\eta}[\sqrt{G}\sin(\phi_1) + g\sqrt{G-1}\sin(\phi_2)]\\ &\approx 2\alpha\sqrt{\eta}(\sqrt{G}\phi_1 + g\sqrt{G-1}\phi_2)\\ &= 2\alpha\sqrt{\eta}(\sqrt{G} + g\sqrt{G-1})\phi, \end{aligned} \tag{A2}$$

$$\begin{aligned}\langle\Delta^2\hat{X}_+\rangle &= \langle\hat{X}_+^2(\phi)\rangle - \langle\hat{X}_+(\phi)\rangle^2\\ &= (g^2+1)(1-2\eta+2\eta G)\\ &\quad - 4g\eta\sqrt{G(G-1)}\cos(\phi_1+\phi 2)\\ &\approx (g^2+1)(1-2\eta+2\eta G) - 4g\eta\sqrt{G(G-1)}, \end{aligned} \tag{A3}$$

where the linear combination of the two measured phases is defined as $\phi = \beta_1\phi_1 + \beta_2\phi_2$, with $\beta_1 = \sqrt{G}/(\sqrt{G} + g\sqrt{G-1})$ and $\beta_2 = g\sqrt{G-1}/(\sqrt{G} + g\sqrt{G-1})$, such that the normalization condition $|\beta_1| + |\beta_2| = 1$ is satisfied. We also assume that the phase shifts ϕ_1 and ϕ_2 are small enough such that the small-angle approximations $\sin(\phi_i) \approx \phi_i$ and $\cos(\phi_1+\phi_2) \approx 1$ can be used. Using Eqs. (A2) and (A3), one can obtain the measurement sensitivity for distributed sensing in a tSU(1,1) interferometer as follows:

$$\begin{aligned}\Delta^2\phi_{\rm tSU} &= \frac{\langle\Delta^2\hat{X}_+\rangle}{(\partial_\phi\langle\hat{X}_+\rangle)^2}\\ &= \frac{(g^2+1)(1-2\eta+2\eta G) - 4g\eta\sqrt{G(G-1)}}{4|\alpha|^2\eta(\sqrt{G}+g\sqrt{G-1})^2}. \end{aligned} \tag{A4}$$

We can compare this result to the fundamental limit given by the QCRB for a two-mode squeezed state in a tSU(1,1) interferometer. Given that the two-mode squeezed state is a Gaussian quantum state, it is completely characterized by displacement vector $\vec{d}$ and covariance matrix σ [55]. The elements of the displacement vector $\vec{d}$ are defined according to $d_i = \langle\hat{A}_i\rangle$, while the ones for the covariance matrix are defined as $\sigma_{i,j} = \langle\hat{A}_i\hat{A}_j^\dagger + \hat{A}_j^\dagger\hat{A}_i\rangle - 2\langle\hat{A}_i\rangle\langle\hat{A}_j^\dagger\rangle$, where $\hat{A} = (\hat{a}_f, \hat{b}_f, \hat{a}_f^\dagger, \hat{b}_f^\dagger)^T$. Note that $\hat{a}_f$ and $\hat{b}_f$ are the modes after the phase elements and losses in Fig. 5(a). In the limit of bright beams, the quantum Fisher information (QFI) takes the form [42,55]

$$F_{i,j} = 2\partial_{\phi_i}\vec{d}^\dagger\sigma^{-1}\partial_{\phi_j}\vec{d}. \tag{A5}$$

Using the QFI, one can show that the QCRB for phase estimation is given by

$$\begin{aligned}\Delta^2\phi_{\rm QCRB} &= (\beta_1 \quad \beta_2)\cdot\vec{F}^{-1}\cdot\begin{pmatrix}\beta_1\\ \beta_2\end{pmatrix}\\ &= \frac{1-2\eta+2\eta G - 2\eta\sqrt{G(G-1)}}{2|\alpha|^2\eta(\sqrt{G}+\sqrt{G-1})^2}. \end{aligned} \tag{A6}$$

From here we can see that $\Delta^2\phi_{\rm QCRB} = \Delta^2\phi_{\rm tSU}$ for $g = 1$. Note that this is the case given that equal losses are considered for the probe and conjugate beams. In this case, the measurement sensitivity of the tSU(1,1) interferometer saturates the QCRB.

Next, we calculate the measurement sensitivity for the corresponding classical configuration using two coherent states, $\hat{a}_c$ and $\hat{b}_c$, to probe the phases elements ϕ_1 and ϕ_2, respectively, as shown in Fig. 5(b). We consider coherent states with the same optical power, $\langle\hat{a}_c^\dagger\hat{a}_c\rangle = G|\alpha|^2$ and $\langle\hat{b}_c^\dagger\hat{b}_c\rangle = (G-1)|\alpha|^2$, as the probe and conjugate in the tSU(1,1) interferometer in the limit of $|\alpha|^2 \gg 1$. Experimentally, an input coherent state $|\gamma\rangle$ is split into two with a beamsplitter to generate beams with the required optical powers. After the phase elements, optical losses are considered with beamsplitter transformations, which leads to $\langle\hat{a}_{cf}^\dagger\hat{a}_{cf}\rangle = \eta G|\alpha|^2$ and $\langle\hat{b}_{cf}^\dagger\hat{b}_{cf}\rangle = \eta(G-1)|\alpha|^2$, respectively. Following the same derivation as the one used to obtain $\Delta^2\phi_{\rm tSU}$, one can show that the expectation value for the joint quadrature operator for the classical distributed sensing case is given by $\langle\hat{X}_{C+}(\phi)\rangle = 2\alpha\sqrt{\eta}(\sqrt{G} + g\sqrt{G-1})\phi$, where $\phi = \beta_1\phi_1 + \beta_2\phi_2$ with the same definition for β_1 and β_2 as used for the tSU(1,1) interferometer. Similarly, the variance can be calculated to be $\langle\Delta^2\hat{X}_{C+}\rangle = (g^2+1)$, which leads to a measurement sensitivity for the classical configuration of the form

$$\Delta^2\phi_{\rm cla} = \frac{g^2+1}{4|\alpha|^2\eta(\sqrt{G}+g\sqrt{G-1})^2}. \tag{A7}$$

Equation (A7) serves as the classical limit to compare with for distributed sensing with the tSU(1,1) interferometer in order to demonstrate a quantum-enhanced sensitivity. Finally, using

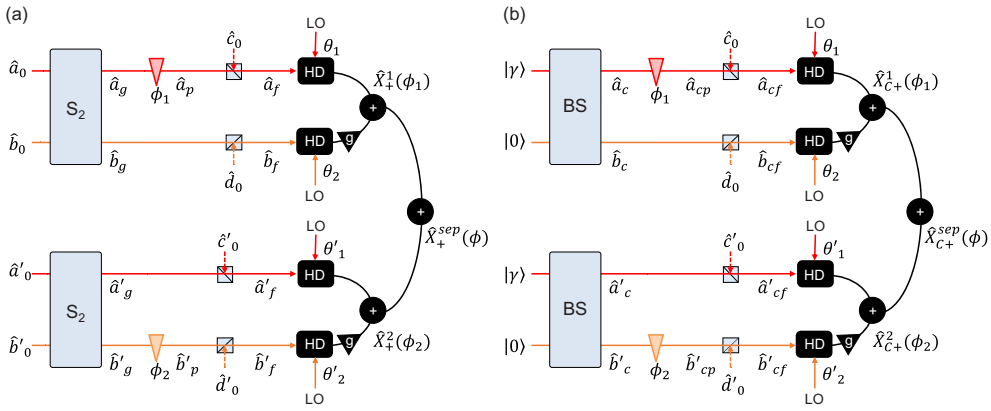

FIG. 6. Schematics for the models considered for the separable sensing configurations when using (a) two tSU(1,1) interferometers and (b) the corresponding classical configuration. The separable sensing configurations that we consider are composed of two interferometers with each one measuring a single phase. S_2: two-mode squeezing operator; BS: beamsplitter.

Eqs. (A4) and (A7), we calculate the range for which the coefficients β_1 and β_2 will still lead to a quantum enhancement. A quantum-enhanced sensitivity can be achieved for β_1 ranging from 0.409 ($\beta_2 = 0.591$) to 0.644 ($\beta_2 = 0.356$) in the lossless case.

APPENDIX B: SEPARABLE CONFIGURATION BASED ON tSU(1,1) INTERFEROMETERS

We now consider the scenario involving the detection of spatially distributed signals, such as gravitational wave detection or ultralight dark matter searches. In these cases, phase shifts are extremely weak and are uniform over extended spatial regions, which makes it worthwhile to consider whether it is more effective to use a single sensing device, like the one we implemented for our experiments on two-phase distributed sensing, or to employ a separable quantum sensing configuration based on the same tSU(1,1) interferometer. For the separable sensing configuration with quantum resources, we consider the case of two tSU(1,1) interferometers with each one measuring a single phase, either ϕ_1 or ϕ_2, as shown in Fig. 6(a). To calculate the phase sensitivity in this case, we can take the results of Appendix A and consider the cases when either one phase or the other is set to zero. For example, for the tSU(1,1) interferometer for which only mode $\hat{a}_g$ experiences a phase shift of ϕ_1, the two output modes would be given by $\hat{a}_p = e^{-i\phi_1}\hat{a}_g$ and $\hat{b}_p = \hat{b}_g$. In this case the generalized measured quadrature takes the form $\hat{X}^1_+(\phi_1) = (-i\hat{a}^\dagger_f + i\hat{a}_f) + g(-i\hat{b}^\dagger_f + i\hat{b}_f)$, which depends only on ϕ_1 through $\hat{a}^\dagger_f$ and $\hat{a}_f$. In the same way, the second tSU(1,1) will lead to a generalized measured quadrature of the form $\hat{X}^2_+(\phi_2) = (-i\hat{a}'^\dagger_f + i\hat{a}'_f) + g(-i\hat{b}'^\dagger_f + i\hat{b}'_f)$, which depends only on ϕ_2 through $\hat{b}'^\dagger_f$ and $\hat{b}'_f$ and where we have assumed that the phases of the LOs are set to $\pi/2$. For this configuration the number of photons probing the phase elements is kept the same as for the distributed case, i.e., $\langle \hat{a}^\dagger_g \hat{a}_g \rangle = \langle \hat{n}_{\rm pr} \rangle$ and $\langle \hat{b}'^\dagger_g \hat{b}'_g \rangle = \langle \hat{n}_{\rm conj} \rangle$ as shown in Fig. 2.

To obtain a measure of the linear combination of the phases, ϕ, we define a joint quadrature operator of the form $\hat{X}^{\rm sep}_+(\phi) = \hat{X}^1_+(\phi_1) + \hat{X}^2_+(\phi_2)$. Through the use of Eqs. (A2) and (A3) we can then show that the expectation value and variance of $\hat{X}^{\rm sep}_+(\phi)$ take the form

$$\begin{aligned}\langle \hat{X}^{\rm sep}_+(\phi)\rangle &= 2\alpha\sqrt{\eta}[\sqrt{G}\sin(\phi_1) + g\sqrt{G-1}\sin(\phi_2)] \\ &\approx 2\alpha\sqrt{\eta}(\sqrt{G}\phi_1 + g\sqrt{G-1}\phi_2) \\ &= 2\alpha\sqrt{\eta}(\sqrt{G} + g\sqrt{G-1})\phi, \end{aligned} \tag{B1}$$

$$\begin{aligned}\langle \Delta^2 \hat{X}^{\rm sep}_+(\phi)\rangle &= 2(g^2+1)(1-2\eta+2\eta G) \\ &\quad - 4g\eta\sqrt{G(G-1)}[\cos(\phi_1) + \cos(\phi_2)] \\ &\approx 2(g^2+1)(1-2\eta+2\eta G) - 8g\eta\sqrt{G(G-1)}, \end{aligned} \tag{B2}$$

where $\phi = \beta_1\phi_1 + \beta_2\phi_2$ and β_1 and β_2 are kept the same as those used in the distributed sensing configurations. With Eqs. (B1) and (B2), one can show that the measurement sensitivity for the separable sensing configuration with two tSU(1,1) interferometers is given by

$$\begin{aligned}\Delta^2\phi^{\rm sep}_{\rm tSU} &= 2\Delta^2\phi_{\rm tSU} \\ &= \frac{(g^2+1)(1-2\eta+2\eta G) - 4g\eta\sqrt{G(G-1)}}{2|\alpha|^2\eta(\sqrt{G}+g\sqrt{G-1})^2}. \end{aligned} \tag{B3}$$

Next, we consider the phase sensitivity for the equivalent classical separable sensing configuration shown in Fig. 6(b). For this, we take coherent states with the same optical power as the probe and conjugate beams used for the two tSU(1,1) interferometers, that is, $\langle \hat{a}^\dagger_c \hat{a}_c \rangle = \langle \hat{a}'^\dagger_c \hat{a}'_c \rangle = G|\alpha|^2$ and $\langle \hat{b}^\dagger_c \hat{b}_c \rangle = \langle \hat{b}'^\dagger_c \hat{b}'_c \rangle = (G-1)|\alpha|^2$ with $|\alpha|^2 \gg 1$. After passing through the phase shifters and considering the losses, one can calculate the measurement sensitivity following the same derivation to show that is given by

$$\Delta^2\phi^{\rm sep}_{\rm cla} = 2\Delta^2\phi_{\rm cla} = \frac{(g^2+1)}{2|\alpha|^2\eta(\sqrt{G}+g\sqrt{G-1})^2}. \tag{B4}$$

There are two things to note for these results. The first is that the separable configuration offers the same degree of quantum enhancement with respect to its corresponding classical

configuration as the distributed one. The second is that the distributed sensing configuration offers a 3 dB SNR improvement over the separable one. It is important to note, however, that this improvement is a classical one that results from the use of additional reference beams for the considered separable sensing configurations.

APPENDIX C: PHASE SENSITIVITY FOR DISTRIBUTED MULTIPHASE SENSING

We generalize the theory for sensing M distributed phases. Here, we only consider the estimation of the average of the phases, i.e., $\phi = \sum_{j=1}^{M} \phi_j/M$, with an assumption that all the phase shifts are small and the same.

1. Classical sensing scheme

For the classical scheme, we consider the case in which an input coherent state with an optical power of $|\gamma|^2$ is divided with a BSN into M modes of the same optical power that are used to probe M unknown phase elements. After the BSN, the average photon number, n, incident on each of the phase elements is given by $n = |\gamma|^2/M$. It has been shown that when n photons are used to sense a phase shift, the sensitivity is given by $\Delta^2\phi_j = 1/(4n)$ when there is a LO with an optical power much larger than n that acts as an external phase reference [56]. Using error propagation, one can readily show that the measurement sensitivity for $\phi = \sum_{j=1}^{M} \phi_j/M$ is given by $\Delta^2\phi_{\rm cla} = 1/(4Mn)$.

2. Separable scheme composed of multiple single-mode squeezed states

An optimal quantum-enhanced separable scheme is obtained when M identical and independent single-mode squeezed states are used to probe the M phase elements. We consider the case in which each single-mode squeezed state has an average photon number of n, such that the resources used to sense each phase are kept constant. In this case, the optimized sensitivity for the separable scheme has been calculated in [24] and is given by

$$\Delta^2\phi_{\rm sep} = \frac{1}{4Mn(n+1)}. \tag{C1}$$

As can be seen, in this case the sensitivity shows a Heisenberg scaling in the number of photons n, but not with the number of modes M.

3. Multimode entangled scheme in a tSU(1,1) interferometer

To generalize the tSU(1,1) used to experimentally sense the average of two phases, we consider a configuration in which the two entangled output modes of a parametric amplifier are split into M entangled modes with a BSN, as shown in Fig. 7. Here, two input modes, $\hat{a}_0$ and $\hat{b}_0$, in vacuum states, i.e., $\langle \hat{a}_0^\dagger \hat{a}_0\rangle = \langle \hat{b}_0^\dagger \hat{b}_0\rangle = 0$, are displaced to become $\hat{a}_1$ and $\hat{b}_1$, respectively, with $\langle \hat{a}_1^\dagger \hat{a}_1\rangle = \langle \hat{b}_1^\dagger \hat{b}_1\rangle = |\alpha|^2$. These displaced modes then serve as the seeds for a parametric amplifier (two-mode squeezer). Note that, as opposed to the experimental implementation in the two-phase case, for this generalized scheme we consider seeding both input modes and assume all

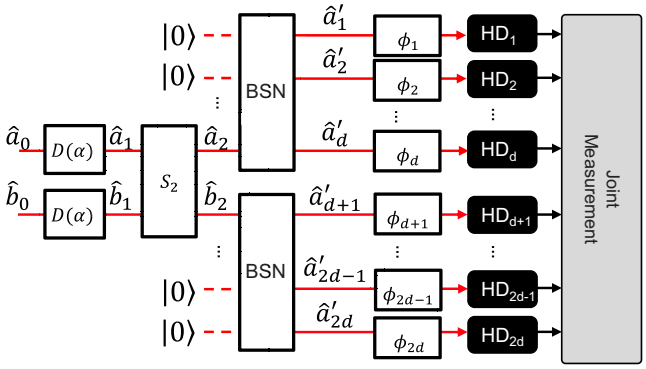

FIG. 7. Generalization to distributed multiphase sensing with a combination of a tSU(1,1) interferometer and a beamsplitter network (BSN). S_2: two-mode squeezing operator.

the involved fields have the same phase. The two output modes of the parametric amplifier, $\hat{a}_2$ and $\hat{b}_2$, follow the same nonlinear gain transformations as the one given in Eq. (A1), such that the total number of photons is given by $N_{\rm tot} = \langle \hat{a}_2^\dagger \hat{a}_2\rangle + \langle \hat{b}_2^\dagger \hat{b}_2\rangle = -2 + 2G + 4G\alpha^2 + 2\alpha^2(-1 + 2\sqrt{G(G-1)})$. After the parametric amplifier, each mode is split into $d = M/2$ modes with a BSN. Each mode is then sent to a single phase element and experiences a phase shift ϕ_j, with the resulting modes labeled as $\hat{a}_j$. For each mode, one can measure the generalized quadrature operator $\hat{X}_j(\phi_j, \theta) = e^{-i\theta}\hat{a}_j^\dagger + e^{i\theta}\hat{a}_j$. We only consider the case in which θ is set to $\pi/2$. Then, the total joint quadrature operator is defined as $\hat{X}_{+,M}(\phi) = \sum_{j=1}^{M} \hat{X}_j(\phi_j)$. The expectation value and variance of this generalized distributed sensor network in the small-angle approximation can be shown to be given by

$$\begin{aligned}\langle \hat{X}_{+,M}(\phi)\rangle &\approx \frac{1}{\sqrt{M}} 2\sqrt{2}\alpha(\sqrt{G} + \sqrt{G-1}) \sum_{j=1}^{M} \phi_j \\ &= 2\sqrt{2}\sqrt{M}\alpha(\sqrt{G} + \sqrt{G-1})\phi, \end{aligned} \tag{C2}$$

$$\langle \Delta^2 \hat{X}_{+,M}(\phi)\rangle \approx M(-1 + 2G - 2\sqrt{G(G-1)}). \tag{C3}$$

Equations (C2) and (C3) can then be used to obtain the measurement sensitivity for the multiphase sensing scheme based on the multimode entangled state obtained with a tSU(1,1) interferometer and a BSN, such that

$$\Delta^2\phi_{\rm ent} = \frac{-1 + 2G - 2\sqrt{G(G-1)}}{8|\alpha|^2(\sqrt{G} + \sqrt{G-1})^2}. \tag{C4}$$

Note that Eq. (C4) does not explicitly depend on the number of modes M. To better compare with the other schemes for multiphase estimation, we use the constraint that the average number of photons hitting each phase element is n, i.e., $N_{\rm tot}/M = \langle \hat{a}_j^\dagger \hat{a}_j\rangle = n$. To optimize the sensitivity for a fixed photon number incident on each phase shifter, we follow the procedure in [24] based on Lagrangian multipliers with this constraint. We can construct the Lagrange function as

$$\mathcal{L}(\alpha, G, \lambda) = \Delta\phi_{\rm ent} + \lambda[(N_{\rm tot}/M) - n]. \tag{C5}$$

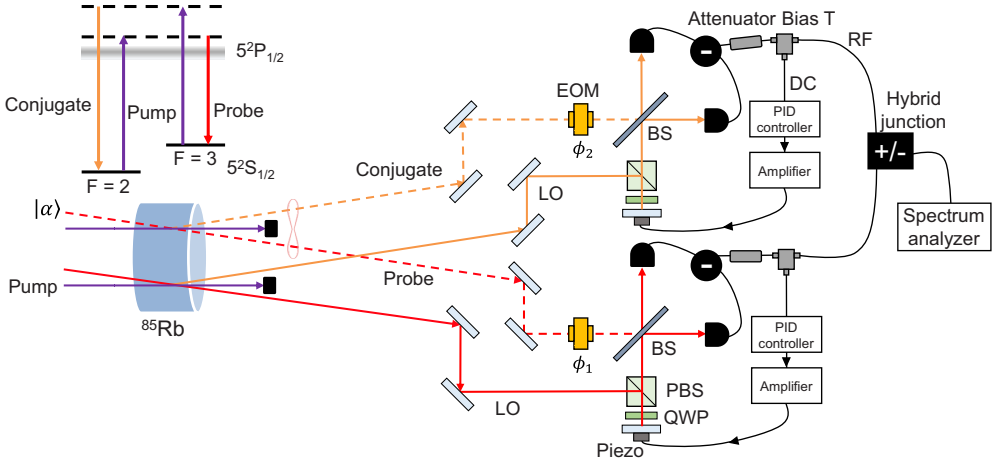

FIG. 8. Experimental setup for the implementation of the distributed two-phase sensing configuration with a tSU(1,1) interferometer. LO: local oscillator; EOM: electro-optic modulator; PBS: polarizing beamsplitter; QWP: quarter waveplate; BS: beamsplitter.

By substituting the solution of Eq. (C5) into Eq. (C4), the optimal measurement sensitivity becomes

$$\Delta^2\phi_{\text{ent}} = \frac{1}{2Mn(Mn+2)}. \tag{C6}$$

As can be seen, for this scheme in which entanglement is distributed to all phase elements, Heisenberg scaling for both the number of photons n and the number of modes M is achieved.

APPENDIX D: EXPERIMENTAL DETAILS

We construct the tSU(1,1) interferometer using a FWM process in a double-lambda configuration in a ^{85}Rb vapor cell, as shown in Fig. 8 [12]. The FWM process is a coherent process in which two photons from a strong pump are absorbed to generate probe and conjugate photons. The frequency of the probe is redshifted by 3.044 GHz with respect to the pump frequency by double passing an acousto-optic modulator (AOM) set to impart a frequency shift of 1.522 GHz. The pump and probe beams are overlapped at an angle of 0.34° in a ^{85}Rb vapor cell with $1/e^2$ beam diameters of 920 μm and 560 μm, respectively. In our configuration, a pump with 360 mW of optical power leads to a FWM with a gain of $G \approx 5$. A spatially separated FWM process in the same vapor cell is used to generate LOs that have the same spatial modes as the probe and conjugate beams for use in the dual balanced homodyne detection. Note that the LOs generated by the FWM are not coherent states. However, to first order, the noise from the LOs does not affect the homodyne detection if the system is properly balanced and has sufficient common mode rejection. Therefore, the two entangled LOs do not affect the measurement of the SNL [45].

For the dual balanced homodyne detection, the probe and conjugate are interfered with their corresponding LOs using a 50:50 beamsplitter and are then measured by a pair of balanced photodetectors (PDs). The PD signals for the probe and conjugate are each sent to an independent variable electronic attenuator to implement the classical gain/attenuation g. Note that we moderately adjusted g to make $\beta_1 = \beta_2 = 1/2$ in the experiment. In order to set the LO phases such that $\theta_1 = \theta_2 = \pi/2$, a bias tee is used to divide the electric signal from each of the PDs into a low frequency (dc) and a high frequency (rf) component with a cutoff frequency of 20 kHz, with the dc component used to lock the difference signal at the zero crossing with a piezodriven mirror. The rf signals, which contain the squeezing and entanglement information, are sent to a hybrid junction to obtain the joint quadrature operators. The hybrid junction outputs both the sum and difference signals of the probe and conjugate homodyne detectors, with the phase sum signal used here.

In order to introduce phase modulations that serve as the signals, two EOMs are driven at a frequency of 300 kHz with independently controlled voltages to implement the different experimental configurations. For the data shown by the red traces in Fig. 3, the EOMs were driven with rf drivers with an applied peak-to-peak voltage of 30 mV, while, for the data shown by the green traces, the peak-to-peak voltage was reduced to 10 mV to impart a smaller signal.

[1] C. M. Caves, Quantum-mechanical noise in an interferometer, Phys. Rev. D **23**, 1693 (1981).
[2] V. Giovannetti, S. Lloyd, and L. Maccone, Quantum-enhanced measurements: Beating the standard quantum limit, Science **306**, 1330 (2004).
[3] S. Pirandola, B. R. Bardhan, T. Gehring, C. Weedbrook, and S. Lloyd, Advances in photonic quantum sensing, Nat. Photon. **12**, 724 (2018).
[4] B. J. Lawrie, P. D. Lett, A. M. Marino, and R. C. Pooser, Quantum sensing with squeezed light, ACS Photon. **6**, 1307 (2019).
[5] L. Pezzè, A. Smerzi, M. K. Oberthaler, R. Schmied, and P. Treutlein, Quantum metrology with nonclassical states of atomic ensembles, Rev. Mod. Phys. **90**, 035005 (2018).
[6] C. L. Degen, F. Reinhard, and P. Cappellaro, Quantum sensing, Rev. Mod. Phys. **89**, 035002 (2017).

[7] C. M. Caves, Reframing SU(1,1) interferometry, Adv. Quantum Technol. **3**, 1900138 (2020).

[8] B. E. Anderson, P. Gupta, B. L. Schmittberger, T. Horrom, C. Hermann-Avigliano, K. M. Jones, and P. D. Lett, Phase sensing beyond the standard quantum limit with a variation on the SU(1,1) interferometer, Optica **4**, 752 (2017).

[9] P. Gupta, B. L. Schmittberger, B. E. Anderson, K. M. Jones, and P. D. Lett, Optimized phase sensing in a truncated SU(1,1) interferometer, Opt. Express **26**, 391 (2018).

[10] N. Prajapati and I. Novikova, Polarization-based truncated SU(1,1) interferometer based on four-wave mixing in Rb vapor, Opt. Lett. **44**, 5921 (2019).

[11] R. C. Pooser and B. Lawrie, Ultrasensitive measurement of microcantilever displacement below the shot-noise limit, Optica **2**, 393 (2015).

[12] R. C. Pooser, N. Savino, E. Batson, J. L. Beckey, J. Garcia, and B. J. Lawrie, Truncated nonlinear interferometry for quantum-enhanced atomic force microscopy, Phys. Rev. Lett. **124**, 230504 (2020).

[13] Y. Xia, A. R. Agrawal, C. M. Pluchar, A. J. Brady, Z. Liu, Q. Zhuang, D. J. Wilson, and Z. Zhang, Entanglement-enhanced optomechanical sensing, Nat. Photon. **17**, 470 (2023).

[14] A. Derevianko, Detecting dark-matter waves with a network of precision-measurement tools, Phys. Rev. A **97**, 042506 (2018).

[15] J. Qin, D. W. P. Amaral, S. A. Bhave, E. Cai, D. Carney, R. F. Lang, S. Li, A. M. Marino, C. Marvinney, J. R. Newton, J. M. Taylor, and C. Tunnell, Mechanical sensors for ultraheavy dark matter searches via long-range forces, arXiv:2503.11645.

[16] P.-A. Moreau, E. Toninelli, T. Gregory, and M. J. Padgett, Imaging with quantum states of light, Nat. Rev. Phys. **1**, 367 (2019).

[17] T. Ono, R. Okamoto, and S. Takeuchi, An entanglement-enhanced microscope, Nat. Commun. **4**, 2426 (2013).

[18] S. Hong, Y.-S. Kim, Y.-W. Cho, S.-W. Lee, H. Jung, S. Moon, S.-W. Han, H.-T. Lim *et al.*, Quantum enhanced multiple-phase estimation with multi-mode N00N states, Nat. Commun. **12**, 5211 (2021).

[19] S. Hong, J. U. Rehman, Y.-S. Kim, Y.-W. Cho, S.-W. Lee, S.-Y. Lee, and H.-T. Lim, Practical sensitivity bound for multiple phase estimation with multi-mode *N*00*N* states, Laser Photon. Rev. **16**, 2100682 (2022).

[20] L. Pezzè and A. Smerzi, Distributed quantum multi-parameter estimation with optimal local measurements, arXiv:2405.18404.

[21] C. M. Gagatsos, D. Branford, and A. Datta, Gaussian systems for quantum-enhanced multiple phase estimation, Phys. Rev. A **94**, 042342 (2016).

[22] Q. Zhuang, Z. Zhang, and J. H. Shapiro, Distributed quantum sensing using continuous-variable multipartite entanglement, Phys. Rev. A **97**, 032329 (2018).

[23] T. J. Proctor, P. A. Knott, and J. A. Dunningham, Multiparameter estimation in networked quantum sensors, Phys. Rev. Lett. **120**, 080501 (2018).

[24] X. Guo, C. R. Breum, J. Borregaard, S. Izumi, M. V. Larsen, T. Gehring, M. Christandl, J. S. Neergaard-Nielsen, and U. L. Andersen, Distributed quantum sensing in a continuous-variable entangled network, Nat. Phys. **16**, 281 (2020).

[25] S.-R. Zhao, Y.-Z. Zhang, W.-Z. Liu, J.-Y. Guan, W. Zhang, C.-L. Li, B. Bai, M.-H. Li, Y. Liu, L. You *et al.*, Field demonstration of distributed quantum sensing without post-selection, Phys. Rev. X **11**, 031009 (2021).

[26] D.-H. Kim, S. Hong, Y.-S. Kim, Y. Kim, R. Lee, S.-W. Lee, R. C. Pooser, K. Oh, S.-Y. Lee, C. Lee, and H.-T. Lim, Distributed quantum sensing of multiple phases with fewer photons, Nat. Commun. **15**, 266 (2024).

[27] Y. Xia, W. Li, W. Clark, D. Hart, Q. Zhuang, and Z. Zhang, Demonstration of a reconfigurable entangled radio-frequency photonic sensor network, Phys. Rev. Lett. **124**, 150502 (2020).

[28] H. Qi, K. Brádler, C. Weedbrook, and S. Guha, Quantum precision of beam pointing, arXiv:1808.01302.

[29] P. Komar, E. M. Kessler, M. Bishof, L. Jiang, A. S. Sørensen, J. Ye, and M. D. Lukin, A quantum network of clocks, Nat. Phys. **10**, 582 (2014).

[30] D. Carney, S. Ghosh, G. Krnjaic, and J. M. Taylor, Proposal for gravitational direct detection of dark matter, Phys. Rev. D **102**, 072003 (2020).

[31] D. Carney, G. Krnjaic, D. C. Moore, C. A. Regal, G. Afek, S. Bhave, B. Brubaker, T. Corbitt, J. Cripe, N. Crisosto *et al.*, Mechanical quantum sensing in the search for dark matter, Quantum Sci. Technol. **6**, 024002 (2021).

[32] A. Attanasio, S. A. Bhave, C. Blanco, D. Carney, M. Demarteau, B. Elshimy, M. Febbraro, M. A. Feldman, S. Ghosh, A. Hickin *et al.*, Snowmass 2021 white paper: The windchime project, arXiv:2203.07242.

[33] F. Hudelist, J. Kong, C. Liu, J. Jing, Z. Ou, and W. Zhang, Quantum metrology with parametric amplifier-based photon correlation interferometers, Nat. Commun. **5**, 3049 (2014).

[34] A. M. Marino, R. C. Pooser, V. Boyer, and P. D. Lett, Tunable delay of Einstein–Podolsky–Rosen entanglement, Nature (London) **457**, 859 (2009).

[35] B. E. Anderson, B. L. Schmittberger, P. Gupta, K. M. Jones, and P. D. Lett, Optimal phase measurements with bright- and vacuum-seeded SU(1,1) interferometers, Phys. Rev. A **95**, 063843 (2017).

[36] S. Liu, Y. Lou, J. Xin, and J. Jing, Quantum enhancement of phase sensitivity for the bright-seeded SU(1,1) interferometer with direct intensity detection, Phys. Rev. Appl. **10**, 064046 (2018).

[37] W. Ge, K. Jacobs, Z. Eldredge, A. V. Gorshkov, and M. Foss-Feig, Distributed quantum metrology with linear networks and separable inputs, Phys. Rev. Lett. **121**, 043604 (2018).

[38] C. Oh, L. Jiang, and C. Lee, Distributed quantum phase sensing for arbitrary positive and negative weights, Phys. Rev. Res. **4**, 023164 (2022).

[39] Y.-Y. Pai, C. E. Marvinney, C. Hua, R. C. Pooser, and B. J. Lawrie, Magneto-optical sensing beyond the shot noise limit, Adv. Quantum Technol. **5**, 2100107 (2022).

[40] C. F. McCormick, V. Boyer, E. Arimondo, and P. D. Lett, Strong relative intensity squeezing by four-wave mixing in rubidium vapor, Opt. Lett. **32**, 178 (2007).

[41] C. F. McCormick, A. M. Marino, V. Boyer, and P. D. Lett, Strong low-frequency quantum correlations from a four-wave-mixing amplifier, Phys. Rev. A **78**, 043816 (2008).

[42] T. S. Woodworth, K. W. C. Chan, C. Hermann-Avigliano, and A. M. Marino, Transmission estimation at the Cramér-Rao bound for squeezed states of light in the presence of loss and imperfect detection, Phys. Rev. A **102**, 052603 (2020).

[43] T. S. Woodworth, C. Hermann-Avigliano, K. W. C. Chan, and A. M. Marino, Transmission estimation at the fundamental

quantum Cramér-Rao bound with macroscopic quantum light, EPJ Quantum Technol. **9**, 38 (2022).

[44] C. You, S. Adhikari, X. Ma, M. Sasaki, M. Takeoka, and J. P. Dowling, Conclusive precision bounds for SU(1,1) interferometers, Phys. Rev. A **99**, 042122 (2019).

[45] V. Boyer, A. M. Marino, R. C. Pooser, and P. D. Lett, Entangled images from four-wave mixing, Science **321**, 544 (2008).

[46] Y. F. Zhou, W. Wang, T. T. Song, X. T. Wang, Q. Q. Zhu, K. Zhang, S. S. Liu, and J. T. Jing, Ultra-large-scale deterministic entanglement containing $2 \times 20\,400$ optical modes based on time-delayed quantum interferometer, Phys. Rev. Lett. **130**, 060801 (2023).

[47] W. Ding, Y.-Y. Wang, S.-F. Gao, M.-L. Wang, and P. Wang, Recent progress in low-loss hollow-core anti-resonant fibers and their applications, IEEE J. Sel. Top. Quantum Electron. **26**, 1 (2020).

[48] S. Kim and A. M. Marino, Atomic resonant single-mode squeezed light from four-wave mixing through feedforward, Opt. Lett. **44**, 4630 (2019).

[49] B. Qi, P. Lougovski, R. Pooser, W. Grice, and M. Bobrek, Generating the local oscillator "locally" in continuous-variable quantum key distribution based on coherent detection, Phys. Rev. X **5**, 041009 (2015).

[50] J. C. Chapman, A. Miloshevsky, H.-H. Lu, N. Rao, M. Alshowkan, and N. A. Peters, Two-mode squeezing over deployed fiber coexisting with conventional communications, Opt. Express **31**, 26254 (2023).

[51] Y. Jeong, C. Lee, and S. Hong, Sensitivity analysis of distributed quantum sensing with a limited squeezing level, in *2024 Conference on Lasers and Electro-Optics Pacific Rim (CLEO-PR)* (IEEE, New York, 2024), pp. 1–2.

[52] R. Pooser and J. Jing, Continuous-variable cluster-state generation over the optical spatial mode comb, Phys. Rev. A **90**, 043841 (2014).

[53] http://energy.gov/downloads/doe-public-access-plan.

[54] M. Jasperse, L. Turner, and R. Scholten, Relative intensity squeezing by four-wave mixing with loss: an analytic model and experimental diagnostic, Opt. Express **19**, 3765 (2011).

[55] D. Šafránek, Estimation of Gaussian quantum states, J. Phys. A: Math. Theor. **52**, 035304 (2019).

[56] M. Jarzyna and R. Demkowicz-Dobrzański, Quantum interferometry with and without an external phase reference, Phys. Rev. A **85**, 011801(R) (2012).